iScience

CellPress
OPEN ACCESS

Article

Inducible deletion of *Ezh2* in CD4$^+$ T cells inhibits kidney T cell infiltration and prevents interstitial nephritis in MRL/*lpr* lupus-prone mice

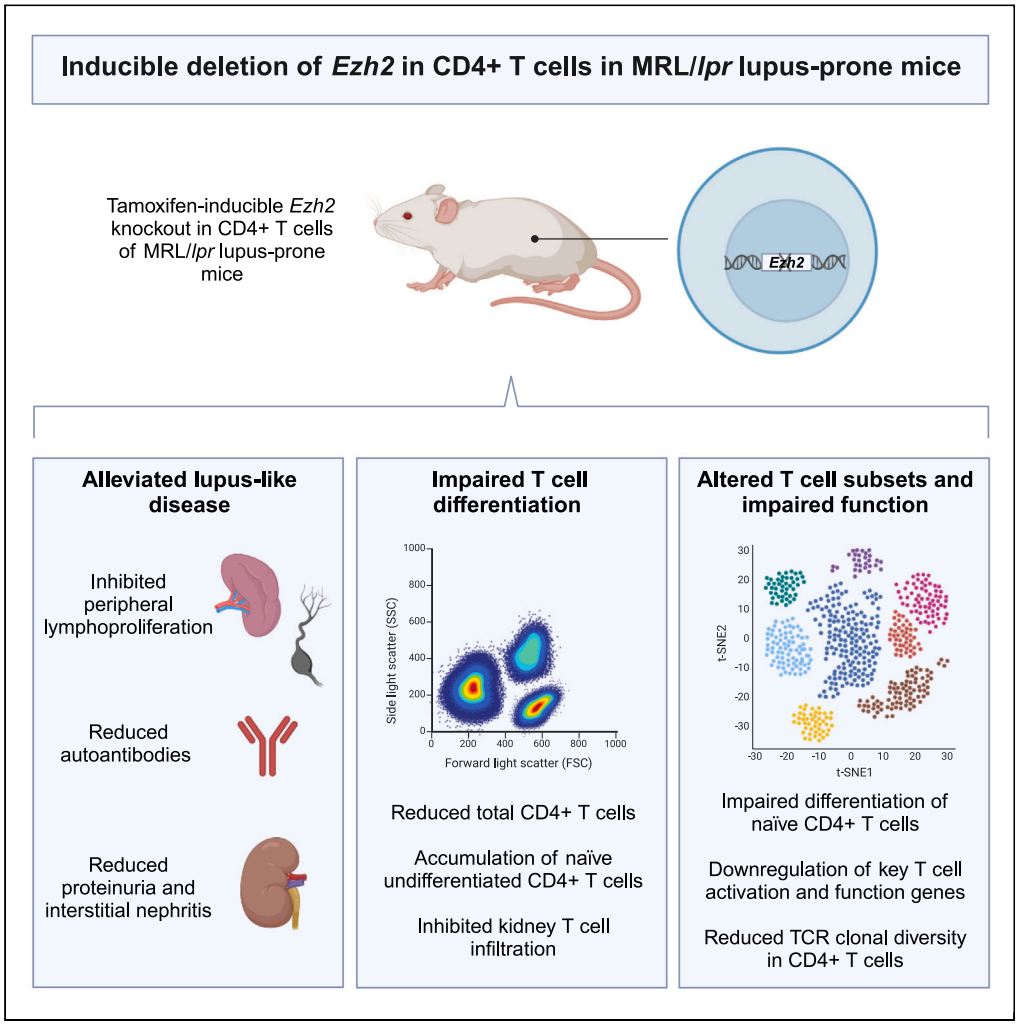

Xiaoqing Zheng, Mikhail G. Dozmorov, Luis Espinoza, Mckenna M. Bowes, Sheldon Bastacky, Amr H. Sawalha

asawalha@pitt.edu

Highlights

CD4+ T cell *Ezh2* deletion prevents lupus and impairs T cell activation

Ezh2 deletion restricts TCR clonal repertoire in the spleen and kidney

EZH2 deficiency inhibits T cell kidney infiltration and interstitial nephritis

Programmed cell death pathways are activated in EZH2-deficient mice

Zheng et al., iScience *27*, 111114
November 15, 2024
https://doi.org/10.1016/j.isci.2024.111114

iScience

CellPress
OPEN ACCESS

Article

Inducible deletion of *Ezh2* in CD4$^+$ T cells inhibits kidney T cell infiltration and prevents interstitial nephritis in MRL/*lpr* lupus-prone mice

Xiaoqing Zheng,[1] Mikhail G. Dozmorov,[2,3] Luis Espinoza,[1] Mckenna M. Bowes,[1] Sheldon Bastacky,[4] and Amr H. Sawalha[1,5,6,7,8,*]

SUMMARY

Systemic lupus erythematosus is a remitting relapsing autoimmune disease characterized by autoantibody production and multi-organ involvement. T cell epigenetic dysregulation plays an important role in the pathogenesis of lupus. We have previously demonstrated upregulation of the key epigenetic regulator EZH2 in CD4$^+$ T cells isolated from lupus patients. To further investigate the role of EZH2 in the pathogenesis of lupus, we generated a tamoxifen-inducible CD4$^+$ T cell *Ezh2* conditional knockout mouse on the MRL/*lpr* lupus-prone background. We demonstrate that *Ezh2* deletion abrogates lupus-like disease and prevents T cell differentiation. Single-cell analysis suggests impaired T cell function and activation of programmed cell death pathways in EZH2-deficient mice. *Ezh2* deletion in CD4$^+$ T cells restricts TCR clonal repertoire and prevents kidney-infiltrating effector CD4$^+$ T cell expansion and tubulointerstitial nephritis, which has been linked to end-stage renal disease in patients with lupus nephritis.

INTRODUCTION

Systemic lupus erythematosus (SLE or lupus) is a heterogeneous remitting-relapsing autoimmune disease that can affect multiple organ systems. Lupus is characterized by autoantibody production, type-I interferon gene expression signature, and DNA methylation defect.[1] Indeed, abnormal T cell DNA methylation is thought to play a central role in the pathogenesis of lupus, in part due to a role for DNA demethylation in inducing T cell autoreactivity.[2] Further, lupus T cells are characterized by robust demethylation of interferon-regulated genes, which precedes T cell activation in lupus patients.[3]

We have previously demonstrated an epigenetic shift in lupus CD4$^+$ T cells that occurs upon increased disease activity. As the disease becomes more active, naive CD4$^+$ T cells are shifted into epigenetic patterns more favorable for proinflammatory T helper cell subsets, and away from differentiation into regulatory T cells.[4] These epigenetic changes occur early in the naive CD4$^+$ T cell stage and precede corresponding transcriptional changes or T cell differentiation. Bioinformatics analysis followed by experimental work suggested that the key epigenetic regulator EZH2 might be underlying the observed disease activity-associated CD4$^+$ T cell epigenetic changes.[4,5] Indeed, we were able to demonstrate increased expression of EZH2 in lupus CD4$^+$ T cells, and that EZH2 overexpression in normal CD4$^+$ T cells leads to proinflammatory epigenetic changes, such as demethylation and overexpression of the adhesion molecule JAM-A.[5] Our work further demonstrated that reduced expression of two microRNAs that regulate EZH2 (miR-101 and miR-26a) underlies EZH2 overexpression in lupus T cells.[5] We further demonstrated that increased glycolysis in lupus T cells explains reduced expression of miR-101 and miR-26a, and that inhibiting glycolysis, either directly or indirectly via blocking mTOR signaling, restores miR-101 and miR-26a levels and inhibits the expression of EZH2.[6]

To demonstrate a pathogenic role for EZH2 in lupus, we treated MRL/*lpr* lupus-prone mice with an EZH2 inhibitor and showed reduced autoantibody production and amelioration of lupus-like disease.[7] To further elucidate the role of EZH2 in lupus CD4$^+$ T cells specifically, we herein generated an MRL/*lpr* mouse with an inducible genetic deletion of *Ezh2* in CD4$^+$ T cells. Using a preventative and a therapeutic model, we show that EZH2 deficiency in CD4$^+$ T cells is sufficient to prevent autoantibody production and improve lupus-like manifestations. We further show that T cell-EZH2 deficiency prevents activation of naive CD4$^+$ T cells and reduces kidney-infiltrating activated T cells as well as interstitial nephritis in MRL/*lpr* mice.

[1]Division of Rheumatology, Department of Pediatrics, Children's Hospital of Pittsburgh, University of Pittsburgh, Pittsburgh, PA, USA
[2]Department of Biostatistics, Virginia Commonwealth University, Richmond, VA, USA
[3]Department of Pathology, Virginia Commonwealth University, Richmond, VA, USA
[4]Department of Pathology, University of Pittsburgh School of Medicine, Pittsburgh, PA, USA
[5]Division of Rheumatology and Clinical Immunology, Department of Medicine, University of Pittsburgh, Pittsburgh, PA, USA
[6]Lupus Center of Excellence, University of Pittsburgh School of Medicine, Pittsburgh, PA, USA
[7]Department of Immunology, University of Pittsburgh, Pittsburgh, PA, USA
[8]Lead contact
*Correspondence: asawalha@pitt.edu
https://doi.org/10.1016/j.isci.2024.111114

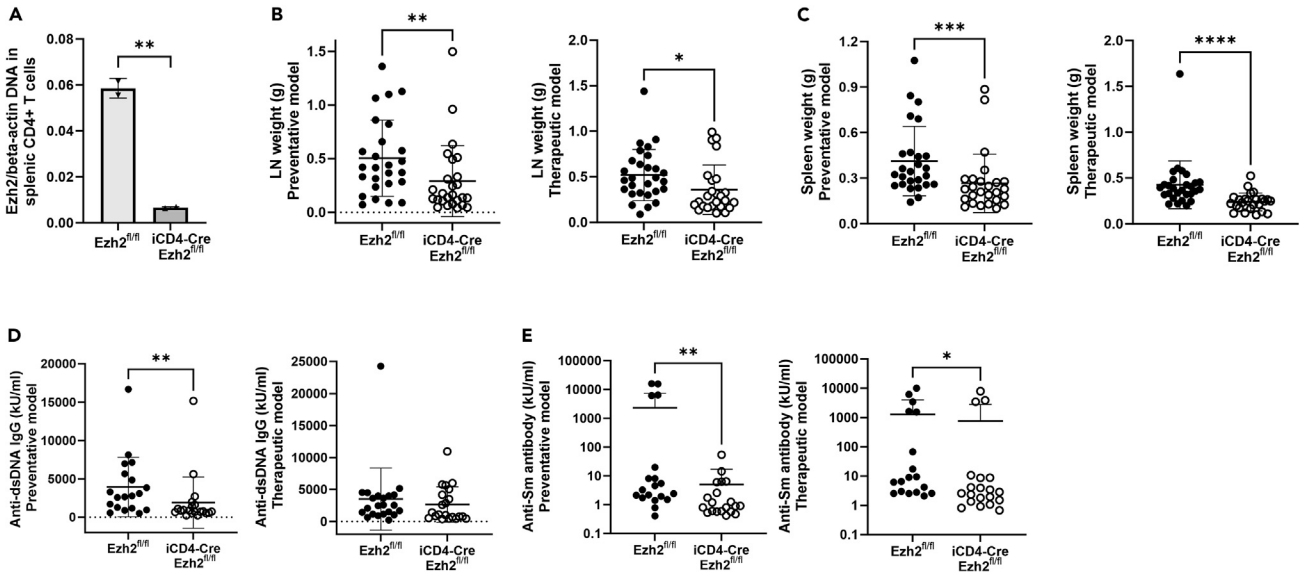

Figure 1. Effect of inducible CD4$^+$ T cell-specific deletion of *Ezh2* in MRL/*lpr* mice

(A) *Ezh2* DNA levels in CD4$^+$ T cells isolated from *Ezh2*$^{fl/fl}$ and CD4-Cre *Ezh2*$^{fl/fl}$ mice after 300 mg/kg tamoxifen treatment for 3 days (Monday, Wednesday, and Friday) by oral gavage. Data are shown as mean ± SD. $^{**}p < 0.01$ ($n = 2$), unpaired two-tailed t-test, t = 17.00, degree of freedom = 2.

(B) Weight of cervical lymph nodes in *Ezh2*$^{fl/fl}$ and iCD4-Cre *Ezh2*$^{fl/fl}$ mice from the preventative and therapeutic mouse models. LN: lymph nodes. Results are presented as mean ± SD, $^{*}p < 0.05$, $^{**}p < 0.01$, two-tailed Mann-Whitney test.

(C) Spleen weight in *Ezh2*$^{fl/fl}$ and iCD4-Cre *Ezh2*$^{fl/fl}$ mice from the preventative and therapeutic mouse models. Data are presented as mean ± SD, $^{***}p < 0.001$, $^{****}p < 0.0001$, two-tailed Mann-Whitney test.

(D and E) Anti-dsDNA IgG and anti-Sm antibody levels in the preventative and therapeutic mouse models. Anti-dsDNA: anti-double stranded DNA. Results are presented as mean ± SD, $^{*}p < 0.05$, $^{**}p < 0.01$, two-tailed Mann-Whitney test.

RESULTS

Tamoxifen-inducible CD4$^+$ T cell-specific deletion of *Ezh2* in MRL/*lpr* mice

We generated a tamoxifen-inducible CD4$^+$ T cell-specific EZH2-deficient mouse (iCD4-Cre *Ezh2*$^{fl/fl}$) on the MRL/*lpr* lupus-prone background. *Ezh2*$^{fl/fl}$ mice without iCD4-Cre were used as controls. Tamoxifen induced *Ezh2* deletion in iCD4-Cre *Ezh2*$^{fl/fl}$ compared to *Ezh2*$^{fl/fl}$ control mice (Figure 1A). No deletion of *Ezh2* was detected in other cell types, including CD8$^+$ T cells (Figure S1).

Ezh2 deletion in CD4$^+$ T cells alleviates lupus-like disease

Ezh2 deletion in CD4$^+$ T cells significantly inhibited peripheral lymphoproliferation, as evidenced by reduced weight of cervical lymph nodes and the spleen in iCD4-Cre *Ezh2*$^{fl/fl}$ compared to *Ezh2*$^{fl/fl}$ control mice in the preventative and therapeutic models (Figures 1B and 1C). These differences were observed in both female and male mice (Figure S2).

The production of anti-dsDNA IgG autoantibody was significantly reduced in EZH2-deficient mice in the preventative but not the therapeutic model (Figure 1D). Anti-Sm autoantibody levels were significantly lower in iCD4-Cre *Ezh2*$^{fl/fl}$ compared to littermate *Ezh2*$^{fl/fl}$ controls in both models (Figure 1E).

We examined the effect of CD4$^+$ T cell-*Ezh2* deletion on lupus nephritis in MRL/*lpr* mice. Urine albumin to creatinine ratio (UACR) was significantly reduced in both the preventative and therapeutic models (Figure 2A). Kidney tissues were fixed, embedded in paraffin, sections were stained with hematoxylin and eosin (H&E), and a renal pathologist reviewed the slides in a blinded manner. Scores were given based on inflammatory changes in the glomeruli and interstitial areas as previously described.[8] EZH2 deficiency in CD4$^+$ T cells did not affect glomerular inflammation (Figure 2B). However, interstitial nephritis was significantly reduced in CD4$^+$ T cell EZH2-deficient mice compared to controls (Figure 2C). Representative kidney H&E staining images from iCD4-Cre *Ezh2*$^{fl/fl}$ and *Ezh2*$^{fl/fl}$ control mice are shown in Figure 2D.

EZH2 deficiency impedes CD4$^+$ T cell activation and differentiation

We observed a significant reduction in CD4$^+$ T cells in the spleen in iCD4-Cre *Ezh2*$^{fl/fl}$ compared to *Ezh2*$^{fl/fl}$ control mice in the preventative model (Figures 3A and 3B). While there was an increase in the percentage of CD8$^+$ T cells in iCD4-Cre *Ezh2*$^{fl/fl}$ mice, there was no significant change in the number of CD8$^+$ T cells in the spleen (Figure 3C). No significant difference was observed in double-negative (CD3ε+ TCRβ+CD4$^-$CD8$^-$) T cells (Figure 3D). Gating strategies are shown in Figure S3.

Among CD4$^+$ T cells in the spleen, the frequency and numbers of naive CD4$^+$ T cells were significantly higher in iCD4-Cre *Ezh2*$^{fl/fl}$ compared to *Ezh2*$^{fl/fl}$ control mice, and CD4$^+$ T cell differentiation into effector memory CD4$^+$ T cells was significantly inhibited with EZH2

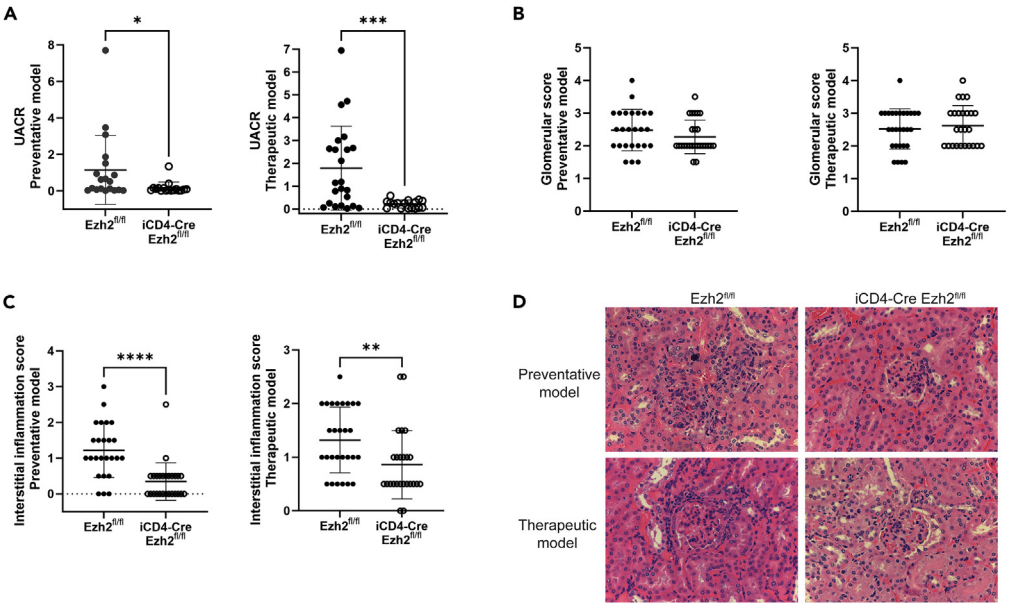

Figure 2. *Ezh2* deletion in CD4$^+$ T cells alleviates lupus nephritis

(A) Urine albumin to creatinine ratio (UACR) in the preventative and therapeutic mouse models. Data are presented as mean ± SD. *$p < 0.05$, ***$p < 0.001$, two-tailed Mann-Whitney test. Glomerulonephritis scores (B) and interstitial nephritis scores (C) in the preventative and therapeutic mouse models. Data are presented as median with interquartile range, **$p < 0.01$, ****$p < 0.0001$, two-tailed Mann-Whitney test.

(D) Representative hematoxylin and eosin (H&E) images of kidney tissues. Original magnification: 400×.

deficiency. Indeed, the majority of CD4$^+$ T cells were naive T cells in iCD4-Cre *Ezh2*$^{fl/fl}$ mice, while there were activated and differentiated into effector memory and central memory CD4$^+$ T cells in *Ezh2*$^{fl/fl}$ control mice (Figures 3E–3H). We also observed a reduction in the number of follicular helper T cells and regulatory CD4$^+$ T cells in EZH2-deficient mice (Figures 3I and 3J). Similar data were obtained from the therapeutic mouse model (Figure S4).

EZH2 deficiency inhibits renal infiltration of CD4$^+$ T cells

We evaluated kidney-infiltrating T cells with and without EZH2 deficiency in the preventative model. We found a significant reduction in kidney-infiltrating T cells in iCD4-Cre *Ezh2*$^{fl/fl}$ compared to control mice, explained by a reduction in CD4$^+$ T cells (Figures 4A–4F). Similar to the spleen, kidney-infiltrating CD4$^+$ T cells from iCD4-Cre *Ezh2*$^{fl/fl}$ mice had significantly fewer central memory and effector memory CD4$^+$ T cells compared to littermate *Ezh2*$^{fl/fl}$ control mice (Figures 4G–4J).

Single-cell RNA-seq reveals T cell subset compositional changes with *Ezh2* deletion

To further explore the effects of EZH2 deficiency in CD4$^+$ T cells, single-cell RNA sequencing (scRNA-seq) was performed in FACS-sorted CD4$^+$ T cells isolated from the spleen. In total, 15 cell populations were clustered based on cell transcriptional profiles. Cell identity of each cluster was determined by evaluating differentially expressed genes within the clusters. We annotated each cluster as demonstrated in Figure 5A, 2 of which were non-T cell clusters (monocytes and macrophages).

We analyzed the proportions of each cell cluster to determine differences in T cell subset composition between iCD4-Cre *Ezh2*$^{fl/fl}$ and control *Ezh2*$^{fl/fl}$ mice. The most significant differences were observed in the proportion of naive and effector CD4$^+$ T cells. iCD4-Cre *Ezh2*$^{fl/fl}$ mice had significantly more naive and less effector CD4$^+$ T cells in the spleen (Figure 5B). Further, iCD4-Cre *Ezh2*$^{fl/fl}$ mice had significantly less late memory CD4$^+$ T cells and follicular helper CD4$^+$ T cells compared to *Ezh2*$^{fl/fl}$ mice (Figure S5).

Our data demonstrate significant impairment in the differentiation of naive CD4$^+$ T cells into effector CD4$^+$ T cells with EZH2 deficiency. To investigate the effect of EZH2 deficiency on the functional status of effector CD4$^+$ T cells as reflected by their transcriptional profile, we compared gene expression profiles in effector CD4$^+$ T cells between iCD4-Cre *Ezh2*$^{fl/fl}$ and control *Ezh2*$^{fl/fl}$ mice. In total, we detected 38 differentially expressed genes, of which 26 and 12 genes were upregulated and downregulated in EZH2-deficient T cells, respectively (Table S1). Gene Ontology analysis focused on Biological Process revealed that 6 out of 12 downregulated genes belong to "positive regulation of leukocyte differentiation" Gene Ontology (GO:1902107, p value = 3.784E-7) (Table S2). These include key genes involved in T cell function, such as *RUNX1*, *IRF1*, *JUN*, *CCR2*, *CCL5*, and *FOS*, which were significantly downregulated in effector CD4$^+$ T cells from iCD4-Cre *Ezh2*$^{fl/fl}$ compared to control *Ezh2*$^{fl/fl}$ mice. Other genes involved in T cell function such as *STAT1* and *LY6A* were also downregulated in EZH2-deficient mice. The negative T cell regulator gene *PDCD1* was significantly upregulated in effector CD4$^+$ T cells in iCD4-Cre

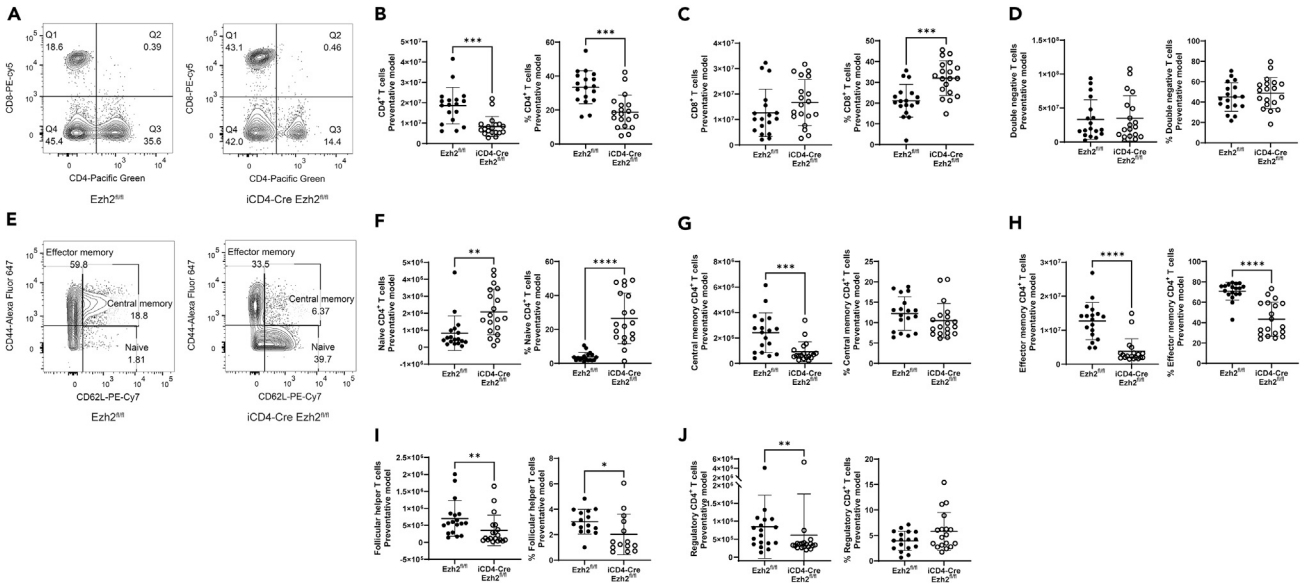

Figure 3. Effect of *Ezh2* deletion on T cell activation and differentiation

Representative flow cytometry plot (A) and statistical analysis of CD4$^+$ T cells (B), CD8$^+$ T cells (C) and double-negative (CD4$^-$CD8$^-$) T cells (D) in the spleen of *Ezh2*$^{fl/fl}$ and iCD4-Cre *Ezh2*$^{fl/fl}$ mice. Representative flow cytometry plot (E) and statistical analysis of naive CD4$^+$ T cells (F), central memory CD4$^+$ T cells (G) and effector memory CD4$^+$ T cells (H) in the spleen of *Ezh2*$^{fl/fl}$ and iCD4-Cre *Ezh2*$^{fl/fl}$ mice. Statistical analysis of follicular helper T cells (I) and regulatory CD4$^+$ T cells (J) in the spleen of *Ezh2*$^{fl/fl}$ and iCD4-Cre *Ezh2*$^{fl/fl}$ mice. Data are presented as mean ± SD. *$p < 0.05$, **$p < 0.01$, ***$p < 0.001$, ****$p < 0.0001$, two-tailed Mann-Whitney test.

Ezh2$^{fl/fl}$ compared to control *Ezh2*$^{fl/fl}$ mice (Figure 5C and Table S1). These data suggest that EZH2 deficiency is associated with reduced numbers and impaired function of effector CD4$^+$ T cells.

To understand what might be driving EZH2-dependent impaired CD4$^+$ T cell transition from naive to effector CD4$^+$ T cells, we compared single-cell transcriptional profiles in naive CD4$^+$ T cells between iCD4-Cre *Ezh2*$^{fl/fl}$ and control *Ezh2*$^{fl/fl}$ mice. We detected 77 differentially expressed genes, of which 23 and 54 genes were upregulated and downregulated in EZH2-deficient T cells, respectively (Table S3). Gene Ontology enrichment analysis revealed enrichment in biological processes involved in protein folding and programmed cell death (Table S4). Further analysis of differentially expressed genes indicates increased entry into the S phase of the cell cycle and suppression of protein transport and key immune-related effector molecules in T cells including cytokine genes such as *IFNG* and *TNF* (Figure S6). Functional annotation also suggested activation of apoptosis (*Z* score = 2.13, *p* = 3.15E-14) in EZH2-deficient T cells.

To examine if EZH2 deficiency altered T cell clonal repertoire, we used TCR RNA-seq to identify the number of TCR alpha-beta clones in iCD4-Cre *Ezh2*$^{fl/fl}$ and control *Ezh2*$^{fl/fl}$ mice. These data reveal a reduction in CD4$^+$ T cell clonal diversity in EZH2-deficient mice, with some clones completely disappearing in iCD4-Cre *Ezh2*$^{fl/fl}$ compared to control *Ezh2*$^{fl/fl}$ mice (Figure 6).

Kidney-infiltrating single-cell RNA-seq reveals T cell subset compositional changes with *Ezh2* deletion

We performed scRNA-seq in FACS-sorted CD4$^+$ T cells isolated from the kidneys of iCD4-Cre *Ezh2*$^{fl/fl}$ and control *Ezh2*$^{fl/fl}$ mice, and identified 12 cell clusters based on transcriptional profiles. Cell identity of each cluster was determined by evaluating differentially expressed genes within the clusters.

These data reveal significant reduction in kidney-infiltrating effector CD4$^+$ T cells in EZH2-deficient mice, consistent with flow cytometry data (Figure S7). Differential gene expression revealed 27 and 18 genes upregulated and downregulated in EZH2-deficient mice, respectively (Table S5). Gene Ontology analysis of downregulated genes revealed a number of biological process ontologies related to T cell activation and function (Table S6). Notably, key genes related to T cell function such as *STAT1*, *CD2*, *CD4*, *CCR2* and *CCR5*, were significantly downregulated in EZH2-deficient kidney-infiltrating effector CD4$^+$ T cells. *PDCD1* was significantly upregulated in kidney-infiltrating effector CD4$^+$ T cells with EZH2 deficiency. Similar to the spleen, CD4$^+$ T cells showed less clonal diversity in EZH2-deficient mice (Figure S7).

DISCUSSION

We generated a mouse model that allows for inducible deletion of *Ezh2* in CD4$^+$ T cells on the MRL/*lpr* lupus-prone genetic background. We demonstrated that inducing EZH2-deficient CD4$^+$ T cells is sufficient to abrogate lupus-like disease. Consistent data were observed when EZH2 deficiency was induced before or after the onset of autoimmunity, in a preventative and a therapeutic *in vivo* model, respectively. We observed significant reduction in proteinuria, and autoantibody production in EZH2-deficient compared to littermate control mice. Interestingly, histological examination showed marked improvement in interstitial nephritis in EZH2-deficient mice, but no difference in

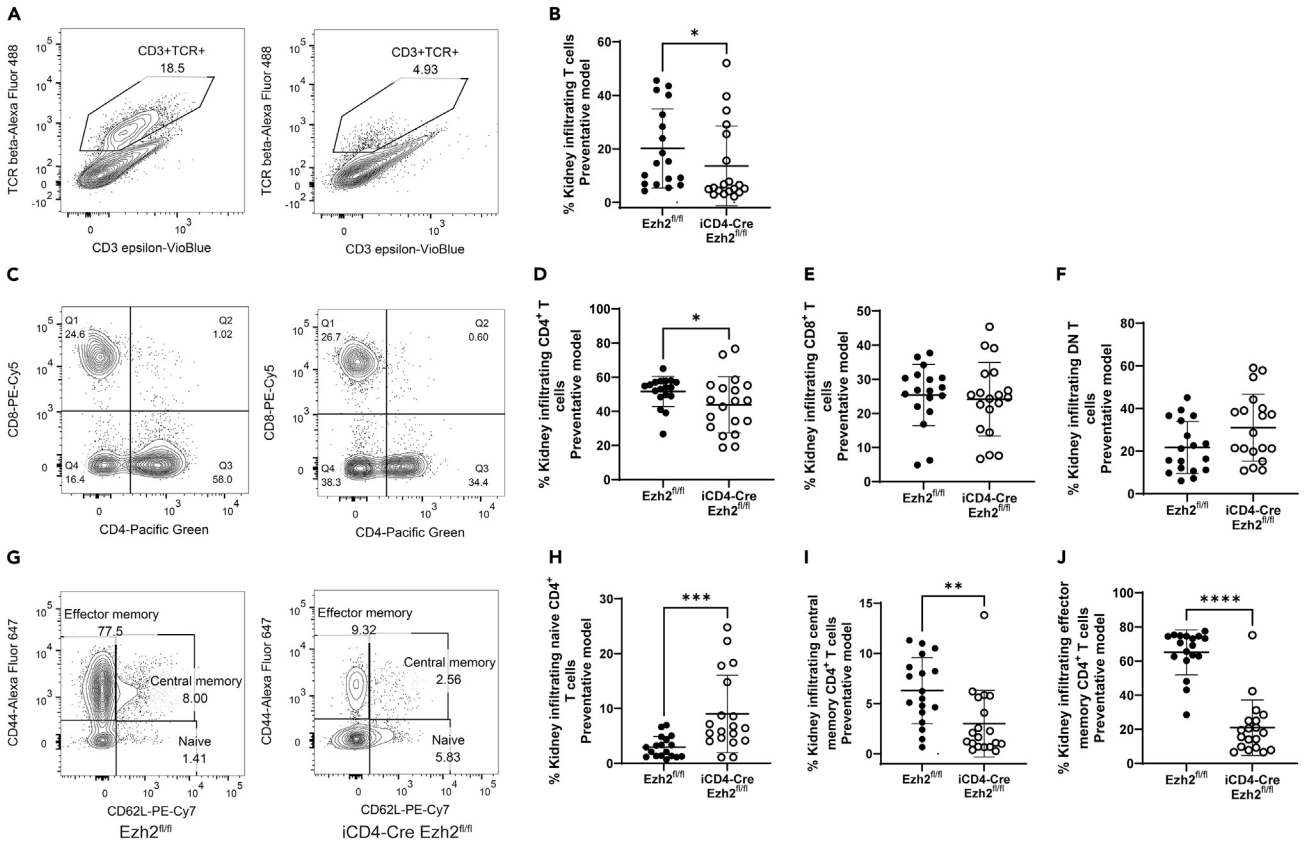

Figure 4. Effect of *Ezh2* deletion on kidney-infiltrating T cells in MRL/*lpr* mice

Representative flow cytometry plot (A) and statistical analysis of (B) kidney-infiltrating CD3ε+ TCRβ+ T cells in *Ezh2*$^{fl/fl}$ and iCD4-Cre *Ezh2*$^{fl/fl}$ mice. Representative flow cytometry plot (C) and statistical analysis of kidney-infiltrating CD4$^+$ T cells (D), CD8$^+$ T cells (E) and double-negative (DN, CD4$^-$CD8$^-$) T cells (F) in *Ezh2*$^{fl/fl}$ and iCD4-Cre *Ezh2*$^{fl/fl}$ mice. Representative flow cytometry plot (G) and statistical analysis of kidney-infiltrating naive CD4$^+$ T cells (H), central memory CD4$^+$ T cells (I) and effector memory CD4$^+$ T cells (J). Data are presented as mean ± SD, *$p < 0.05$, **$p < 0.01$, ***$p < 0.001$, ****$p < 0.0001$, two-tailed Mann-Whitney test.

glomerulonephritis scores between iCD4-Cre *Ezh2*$^{fl/fl}$ and *Ezh2*$^{fl/fl}$ control mice. This is in contrast to the effects we previously observed when we deleted *Ezh2* in B cells in MRL/*lpr* mice. Indeed, mice with EZH2-deficiency in B cells demonstrated impaired germinal center B cell and plasmablast differentiation, and had significant reduction in proteinuria but with histological improvement in glomerulonephritis and no effect on interstitial nephritis.[9] Taken together, these data suggest that EZH2 deficiency induces distinct cell-type specific but complementary effects on renal involvement in MRL/*lpr* mice. While immune-complex deposition and the resulting glomerulonephritis is the whole mark of lupus nephritis, strong evidence suggests that interstitial nephritis is a predictor of progression to end-stage renal disease in lupus patients.[10,11] We observed a significant reduction in kidney-infiltrating effector CD4$^+$ T cells in EZH2-deficient mice. Further, scRNA-seq of kidney-infiltrating CD4$^+$ T cells revealed a transcriptional profile consistent with impaired T cell function in iCD4-Cre *Ezh2*$^{fl/fl}$ compared to *Ezh2*$^{fl/fl}$ control mice.

Our data revealed that deleting *Ezh2* in CD4$^+$ T cells impairs T cell differentiation and activation in MRL/*lpr* mice. Flow cytometry and scRNA-seq data confirmed significant reduction in effector CD4$^+$ T cells and the accumulation of naive CD4$^+$ T cells in the spleen of EZH2-deficient compared to control mice. Furthermore, analysis of kidney-infiltrating T cells revealed a significant reduction in effector CD4$^+$ T cells in EZH2-deficient mice. ScRNA-seq of the T cell receptor suggests a polyclonal effect of EZH2 deficiency, with evidence of reduced numbers of T cell clonotypes and deletion of T cell clones in both the spleen and in kidney-infiltrating CD4$^+$ T cells in iCD4-Cre *Ezh2*$^{fl/fl}$ compared to *Ezh2*$^{fl/fl}$ control mice. The specificities of the deleted T cell clones and whether they are autoreactive remains to be determined.

EZH2 expression has been shown to be play an important role in T cell development and function.[12] Studies in tumor-infiltrating T cells suggest that EZH2-expressing CD4$^+$ T cells are pro-inflammatory and characterized by polyfunctional cytokine expression.[13] They are capable of expressing multiple cytokines, including IL-2, interferon-γ, and TNF.[13] It has been suggested that EZH2 induces T cell activation by repressing Notch signaling repressor genes *Numb* and *Fbxw7*.[13] We did not observe differential expression of *Numb* or *Fbxw7* in iCD4-Cre *Ezh2*$^{fl/fl}$ compared to *Ezh2*$^{fl/fl}$ control MRL/*lpr* mice. However, scRNA-seq analysis in effector CD4$^+$ T cells in the spleen revealed downregulation of

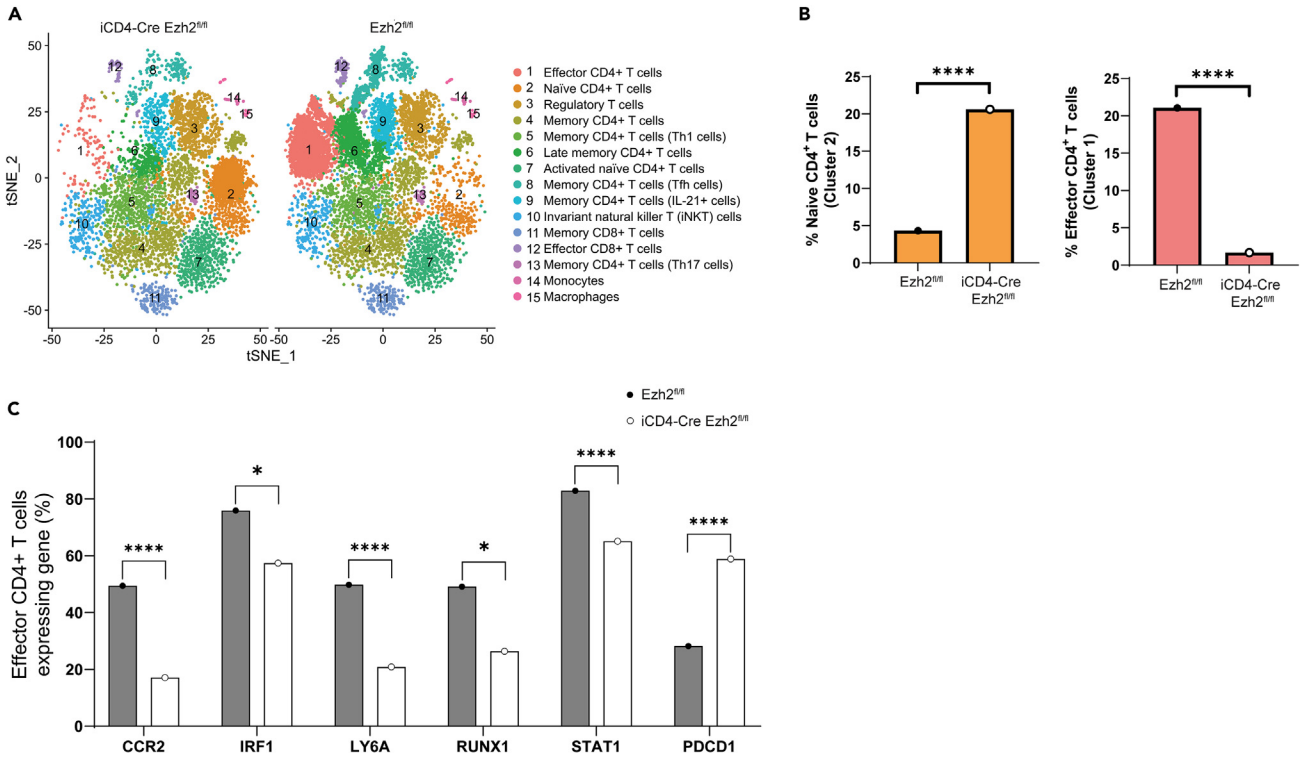

Figure 5. Single-cell RNA-sequencing of CD4$^+$ T cells isolated from the spleen in female *Ezh2$^{fl/fl}$* and iCD4-Cre *Ezh2$^{fl/fl}$* mice from the preventative model

(A) tSNE plot of cell clusters identified.

(B) Frequency of naive CD4$^+$ T cells and effector CD4$^+$ T cells in *Ezh2$^{fl/fl}$* and iCD4-Cre *Ezh2$^{fl/fl}$* mice. ****$p < 0.0001$, proportion test.

(C) Proportion of effector CD4$^+$ T cells expressing indicated genes in *Ezh2$^{fl/fl}$* and iCD4-Cre *Ezh2$^{fl/fl}$* mice. *$p < 0.05$, ****$p < 0.0001$, proportion test.

several key genes involved in T cell function in EZH2-deficient mice. These include *RUNX1*, *IRF1*, *JUN*, *CCR2*, *CCL5*, and *FOS*, which are involved in T cell proliferation, activation, migration, differentiation, and cytokine production.[14–18] These data suggest that impaired differentiation and function of effector CD4$^+$ T cells underlies improvement of lupus-like disease in EZH2-deficient mice. Indeed, downregulation of *CCR2*/*CCL5*, which play a role in T cell migration, might explain significantly reduced abundance of effector CD4$^+$ T cells in the kidneys of EZH2-deficient mice.

To gain further insights into possible mechanisms underlying impaired T cell differentiation from naive to effector CD4$^+$ T cells in EZH2-deficient mice, we compared gene expression profiles in naive CD4$^+$ T cells between iCD4-Cre *Ezh2$^{fl/fl}$* and control *Ezh2$^{fl/fl}$* mice. Functional bioinformatics analysis suggests that EZH2 deficiency favors the entry of naive CD4$^+$ T cells into the S phase of the cell cycle and the activation of programmed cell death pathways. This is consistent with previous reports suggesting that EZH2 expression in T cells confers resistance to apoptosis.[13,19] Further, the negative T cell regulator gene *PDCD1* was upregulated in effector CD4$^+$ T cells in both the spleen and the kidney in EZH2-deficient mice.

In summary, our data provide additional support for the role of EZH2 in autoimmunity and the potential therapeutic implications of targeting EZH2 in lupus. Enhancing CD4$^+$ T cell entry into the S phase of the cell cycle, activation of programmed cell death, and reduced effector T cell function by suppressing key T cell transcriptional regulators appear to mediate the potential therapeutic effect of inhibiting EZH2 in the setting of autoimmunity. Importantly, T cell EZH2 deficiency prevents the accumulation of effector CD4$^+$ T cells in the kidneys and the development of tubulointerstitial nephritis which is a strong predictor of end-stage renal disease in patients with lupus nephritis. Further studies to explore the repurposing of EZH2 inhibitors in the setting of clinical trials in lupus nephritis are warranted.

Limitations of the study

The study focused on CD4$^+$ T cells, and exploring the effect of EZH2 deficiency in other T cell subtypes might add additional insights into the role of EZH2 in lupus. Further, this study was performed in MRL/*lpr* lupus-prone mice, and while this mouse model develops lupus-like manifestations that closely resemble human lupus, expanding our studies to other lupus mouse models might be warranted. In addition, future studies to explore long-term effects of *Ezh2* deletion can help to understand durability of the therapeutic benefits and potential adverse effects. Furthermore, given that EZH2 is overexpressed in T cells from lupus patients, there is a need for studies investigating the effects of EZH2 overexpression in animal models to fully understand the role of EZH2 in lupus T cells.

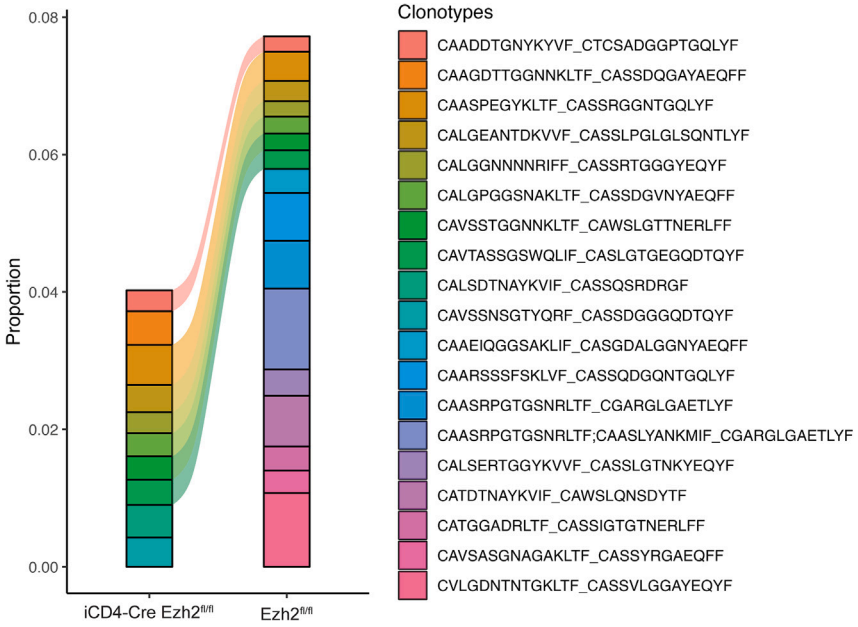

Figure 6. T cell receptor (TCR) repertoire analysis in the spleen using single-cell TCR RNA-sequencing in *Ezh2*$^{fl/fl}$ and iCD4-Cre *Ezh2*$^{fl/fl}$ mice

RESOURCE AVAILABILITY

Lead contact

Further information and requests for resources and reagents should be directed to and will be fulfilled by the lead contact, Dr. Amr H Sawalha (asawalha@pitt.edu).

Materials availability

This study did not generate new unique reagents.

Data and code availability

- Single-cell RNA-seq data reported in this paper have been deposited in Gene Expression Omnibus, with the accession number listed in the key resources table.
- This paper does not report original code.
- Any additional information required to reanalyze the data reported in this paper is available from the lead contact upon request.

ACKNOWLEDGMENTS

This work was supported by the National Institute of Allergy and Infectious Diseases (NIAID) of the National Institutes of Health (NIH) grant number R01 AI097134. We are thankful to Dr. Jeremy Tilstra for his advice in isolating kidney-infiltrating T cells, and Dr. Desiré Casares-Marfil and Dr. Huizhong Long for their help with this manuscript.

AUTHOR CONTRIBUTIONS

X.Z.: Conducting experiments, acquiring data, analyzing data, contributed to writing the manuscript; M.G.D.: Analyzing data, contributed to writing the manuscript; L.E.: Conducting experiments, acquiring data. M.M.B.: Conducting experiments, acquiring data; S.B.: Analyzing data; A.H.S.: Designing research studies, analyzing data, writing the manuscript.

DECLARATION OF INTERESTS

None of the authors report any relevant financial conflict of interest. X.Z. is currently employed as a scientist at The Jackson Laboratory.

STAR★METHODS

Detailed methods are provided in the online version of this paper and include the following:

- KEY RESOURCES TABLE
- EXPERIMENTAL MODEL AND STUDY PARTICIPANT DETAILS
- METHOD DETAILS
  - Spleen and lymph node weight
  - Plasma autoantibody measurements

- Proteinuria and nephritis assessment
- Single-cell RNA sequencing (scRNA-seq) and single-cell T-cell receptor sequencing (scTCR-seq) of splenic $CD4^+$ T cells and kidney-infiltrating $CD4^+$ T cells
- Single-cell sequencing data analysis
- Flow cytometry analysis of $CD4^+$ T cells

- QUANTIFICATION AND STATISTICAL ANALYSIS

SUPPLEMENTAL INFORMATION

Supplemental information can be found online at https://doi.org/10.1016/j.isci.2024.111114.

Received: July 5, 2024
Revised: August 20, 2024
Accepted: October 3, 2024
Published: October 9, 2024

REFERENCES

1. Tsokos, G.C. (2020). Autoimmunity and organ damage in systemic lupus erythematosus. Nat. Immunol. *21*, 605–614.
2. Zheng, X., and Sawalha, A.H. (2022). The Role of Oxidative Stress in Epigenetic Changes Underlying Autoimmunity. Antioxidants Redox Signal. *36*, 423–440.
3. Coit, P., Jeffries, M., Altorok, N., Dozmorov, M.G., Koelsch, K.A., Wren, J.D., Merrill, J.T., McCune, W.J., and Sawalha, A.H. (2013). Genome-wide DNA methylation study suggests epigenetic accessibility and transcriptional poising of interferon-regulated genes in naive CD4+ T cells from lupus patients. J. Autoimmun. *43*, 78–84.
4. Coit, P., Dozmorov, M.G., Merrill, J.T., McCune, W.J., Maksimowicz-McKinnon, K., Wren, J.D., and Sawalha, A.H. (2016). Epigenetic Reprogramming in Naive CD4+ T Cells Favoring T Cell Activation and Non-Th1 Effector T Cell Immune Response as an Early Event in Lupus Flares. Arthritis Rheumatol. *68*, 2200–2209.
5. Tsou, P.S., Coit, P., Kilian, N.C., and Sawalha, A.H. (2018). EZH2 Modulates the DNA Methylome and Controls T Cell Adhesion Through Junctional Adhesion Molecule A in Lupus Patients. Arthritis Rheumatol. *70*, 98–108.
6. Zheng, X., Tsou, P.S., and Sawalha, A.H. (2020). Increased Expression of EZH2 Is Mediated by Higher Glycolysis and mTORC1 Activation in Lupus CD4(+) T Cells. Immunometabolism *2*, e200013.
7. Rohraff, D.M., He, Y., Farkash, E.A., Schonfeld, M., Tsou, P.S., and Sawalha, A.H. (2019). Inhibition of EZH2 Ameliorates Lupus-Like Disease in MRL/lpr Mice. Arthritis Rheumatol. *71*, 1681–1690.
8. Tilstra, J.S., John, S., Gordon, R.A., Leibler, C., Kashgarian, M., Bastacky, S., Nickerson, K.M., and Shlomchik, M.J. (2020). B cell-intrinsic TLR9 expression is protective in murine lupus. J. Clin. Invest. *130*, 3172–3187.
9. Zheng, X., Dozmorov, M.G., Strohlein, C.E., Bastacky, S., and Sawalha, A.H. (2023). Ezh2 Knockout in B Cells Impairs Plasmablast Differentiation and Ameliorates Lupus-like Disease in MRL/lpr Mice. Arthritis Rheumatol. *75*, 1395–1406.
10. Hsieh, C., Chang, A., Brandt, D., Guttikonda, R., Utset, T.O., and Clark, M.R. (2011). Predicting outcomes of lupus nephritis with tubulointerstitial inflammation and scarring. Arthritis Care Res. *63*, 865–874.
11. Yu, F., Wu, L.H., Tan, Y., Li, L.H., Wang, C.L., Wang, W.K., Qu, Z., Chen, M.H., Gao, J.J., Li, Z.Y., et al. (2010). Tubulointerstitial lesions of patients with lupus nephritis classified by the 2003 International Society of Nephrology and Renal Pathology Society system. Kidney Int. *77*, 820–829.
12. Nutt, S.L., Keenan, C., Chopin, M., and Allan, R.S. (2020). EZH2 function in immune cell development. Biol. Chem. *401*, 933–943.
13. Zhao, E., Maj, T., Kryczek, I., Li, W., Wu, K., Zhao, L., Wei, S., Crespo, J., Wan, S., Vatan, L., et al. (2016). Cancer mediates effector T cell dysfunction by targeting microRNAs and EZH2 via glycolysis restriction. Nat. Immunol. *17*, 95–103.
14. Korinfskaya, S., Parameswaran, S., Weirauch, M.T., and Barski, A. (2021). Runx Transcription Factors in T Cells-What Is Beyond Thymic Development? Front. Immunol. *12*, 701924.
15. Mamane, Y., Heylbroeck, C., Génin, P., Algarté, M., Servant, M.J., LePage, C., DeLuca, C., Kwon, H., Lin, R., and Hiscott, J. (1999). Interferon regulatory factors: the next generation. Gene *237*, 1–14.
16. Shah, K., Al-Haidari, A., Sun, J., and Kazi, J.U. (2021). T cell receptor (TCR) signaling in health and disease. Signal Transduct. Targeted Ther. *6*, 412.
17. Heng, A.H.S., Han, C.W., Abbott, C., McColl, S.R., and Comerford, I. (2022). Chemokine-Driven Migration of Pro-Inflammatory CD4(+) T Cells in CNS Autoimmune Disease. Front. Immunol. *13*, 817473.
18. Zeng, Z., Lan, T., Wei, Y., and Wei, X. (2022). CCL5/CCR5 axis in human diseases and related treatments. Genes Dis. *9*, 12–27.
19. Zhang, Y., Kinkel, S., Maksimovic, J., Bandala-Sanchez, E., Tanzer, M.C., Naselli, G., Zhang, J.G., Zhan, Y., Lew, A.M., Silke, J., et al. (2014). The polycomb repressive complex 2 governs life and death of peripheral T cells. Blood *124*, 737–749.
20. Choi, J.H., In Kim, H., and Woo, H.G. (2020). scTyper: a comprehensive pipeline for the cell typing analysis of single-cell RNA-seq data. BMC Bioinf. *21*, 342.
21. Aran, D., Looney, A.P., Liu, L., Wu, E., Fong, V., Hsu, A., Chak, S., Naikawadi, R.P., Wolters, P.J., Abate, A.R., et al. (2019). Reference-based analysis of lung single-cell sequencing reveals a transitional profibrotic macrophage. Nat. Immunol. *20*, 163–172.

STAR★METHODS

KEY RESOURCES TABLE

REAGENT or RESOURCE	SOURCE	IDENTIFIER
Antibodies		
Anti-CD3 epsilon-VioBlue (Clone 17A2)	Miltenyi Biotec	Cat#130-118-849
Anti-TCR β-Alexa Fluor 488 (Clone H57-597)	BioLegend	Cat#109215
Anti-CD4-Pacific Green (Clone RM4-5)	Thermo Fisher Scientific	Cat#C11207
Anti-FoxP3-PE (Clone REA788)	Miltenyi Biotec	Cat#130-111-678
Anti-CD44-Alexa Fluor 647 (Clone IM7)	BioLegend	Cat#103017
Anti-CD62L-PE/Cyanine7 (Clone MEL-14)	BioLegend	Cat#104417
Anti-CD185 (CXCR5)-PerCP/Cyanine5.5 (Clone L138D7)	BioLegend	Cat#145507
Anti-CD279 (PD1)-PE-Dazzle 594 (Clone RMP1-30)	BioLegend	Cat#109115
Anti-mouse CD16/CD32	BD Biosciences	Cat#553142
Anti-CD8a-PE-Cyanine5 (Clone 53-6.7)	BioLegend	Cat#100710
Chemicals, peptides, and recombinant proteins		
Tamoxifen	Sigma-Aldrich	T5648
Critical commercial assays		
LIVE/DEAD™ Fixable Near-IR Dead Cell Stain Kit	Thermo Fisher Scientific	Cat#L34976
True-Nuclear Transcription Factor Buffer Set	BioLegend	Cat#424401
Mouse anti-dsDNA IgG-specific ELISA Kit	Alpha Diagnostic International	Cat#5120
Mouse Anti-Sm Ig's (total (A+G+M) ELISA Kit	Alpha Diagnostic International	Cat#5405
Mouse Albumin ELISA Kit	Alpha Diagnostic International	Cat#6300
Creatinine Parameter Assay Kit	R&D Systems	Cat#KGE005
Multi Tissue Dissociation Kit 2	Miltenyi Biotec	Cat#130-110-203
Experimental models: Organisms/strains		
B6(129X1)-Tg(Cd4-cre/ERT2)11Gnri/J	Jackson Laboratory	Strain#022356
MRL/*lpr*	Jackson Laboratory	Strain#000480
Software and algorithms		
GraphPad Prism 9.2.0	GraphPad	N/A
Cell Ranger v. 7.1.0	10x Genomics	N/A
Deposited data		
Single-cell RNA sequencing data	This paper	GEO#GSE278393

EXPERIMENTAL MODEL AND STUDY PARTICIPANT DETAILS

Female B6(129X1)-Tg(Cd4-cre/ERT2)11Gnri/J mice from the Jackson Laboratory were backcrossed to MRL/*lpr* male mice. A speed congenic method was used by selecting the top two out of 15-20 male pups with the highest MRL/*lpr* genetic background from each generation for subsequent backcrossing. After 6 generations, a mouse reached 99.8% MRL/*lpr* background and was crossed with female *EZH2*$^{fl/fl}$ MRL/*lpr* mice we recently generated,[9] to get *Ezh2*$^{fl/fl}$ and CD4-Cre/ERT2 *Ezh2*$^{fl/fl}$ (abbreviated as iCD4-Cre *Ezh2*$^{fl/fl}$) mice. Both groups of mice received oral gavage administration of tamoxifen (300 mg/Kg) dissolved in corn oil 3 days a week (on Mondays, Wednesdays and Fridays), every other week starting from 10 weeks of age in the preventative model and 14 weeks of age in the therapeutic model until mice reached 24 weeks of age. The *Ezh2*$^{fl/fl}$ and littermate iCD4-Cre *Ezh2*$^{fl/fl}$ mice were housed together in a pathogen-free environment. Upon euthanasia, we isolated superficial and deep cervical lymph nodes, spleens, and kidneys. All animal work has been approved by the University of Pittsburgh Institutional Animal Care and Use Committee (IACUC Protocol #22081569).

METHOD DETAILS

Spleen and lymph node weight

Following mouse euthanasia, we isolated and weighed superficial and deep cervical lymph nodes as well as the spleens using the following number of mice: preventative model, n= 26 mice for iCD4-Cre *Ezh2*$^{fl/fl}$ group and n= 26 mice for *Ezh2*$^{fl/fl}$ group; therapeutic model, n= 25 mice for iCD4-Cre *Ezh2*$^{fl/fl}$ group and n= 28 mice for *Ezh2*$^{fl/fl}$ group.

Plasma autoantibody measurements

Following mouse euthanasia, cardiac puncture was performed to collect blood in K2EDTA tubes. Plasma was isolated by centrifuging at 1500 rcf for 15 minutes, and stored at -80°C. We measured plasma levels of anti-doubled-stranded (anti-dsDNA) IgG and anti-Sm antibodies using an ELISA method, following the manufacturer's instructions (Alpha Diagnostic International, San Antonio, USA). The following number of mice were used: anti-dsDNA IgG (preventative model), n= 20 mice for iCD4-Cre *Ezh2*$^{fl/fl}$ group and n= 19 mice for *Ezh2*$^{fl/fl}$ group; anti-dsDNA IgG (therapeutic model), n= 21 mice for iCD4-Cre *Ezh2*$^{fl/fl}$ group and n= 22 mice for *Ezh2*$^{fl/fl}$ group; anti-Sm antibody (preventative model), n= 20 mice for iCD4-Cre *Ezh2*$^{fl/fl}$ group and n= 19 mice for *Ezh2*$^{fl/fl}$ group; anti-Sm antibody (therapeutic model), n= 20 mice for iCD4-Cre *Ezh2*$^{fl/fl}$ group and n= 18 mice for *Ezh2*$^{fl/fl}$ group.

Proteinuria and nephritis assessment

Mouse urine was collected less than a week before euthanasia and stored at -80°C. Urine albumin (Alpha Diagnostic International, San Antonio, USA) and creatinine (R&D Systems, Minneapolis, USA) were measured following the kit instructions. Urine albumin to creatinine ratio (UACR) was used to evaluate proteinuria. The following number of mice were used for proteinuria assessment: preventative model, n= 17 mice for iCD4-Cre *Ezh2*$^{fl/fl}$ group and n= 19 mice for *Ezh2*$^{fl/fl}$ group; therapeutic model, n= 17 mice for iCD4-Cre *Ezh2*$^{fl/fl}$ group and n= 23 mice for *Ezh2*$^{fl/fl}$ group.

One kidney from each mouse, after capsule removal, was fixed in formalin, and stored in 70% ethanol before paraffin embedding, sectioning, and staining with hematoxylin and eosin (H&E). Kidney H&E stained slides were then reviewed by a renal pathologist in a blinded manner. Inflammation in glomeruli and interstitial areas was quantitatively scored as previously described.[8] Specifically, glomerulonephritis was evaluated using a scale from 1 to 6 as follows: 1 represents a normal kidney; 2 indicates mesangial expansion with increased cellularity and patent capillary loops; 3 reflects enlarged glomeruli with moderate endocapillary hypercellularity; 4 includes the characteristics of grade 3 with significant endocapillary hypercellularity and the loss of patency in most capillary loops; 5 indicates the presence of a few glomeruli with necrosis (karyorrhexis) or a small number of active (cellular or fibrocellular) or organized (fibrous) crescents; and 6 is characterized by numerous active (cellular or fibrocellular) or organized (fibrous) crescents, necrosis (karyorrhexis), obliteration of glomerular architecture, and segmental or global sclerosis. Interstitial nephritis was assessed on a 1 to 4 scale as follows: 1 denotes minimal inflammation (lymphocytes and plasma cells) confined to the perivascular area; 2 involves expansion of inflammation throughout the interstitial space but confined to a discrete area; 3 indicates diffuse infiltrates in more than 40% of high-power fields; and 4 represents diffuse infiltration throughout the entire interstitial space.[8] The following number of mice were used for histological assessment: preventative model, n= 26 mice for iCD4-Cre *Ezh2*$^{fl/fl}$ group and n= 25 mice for *Ezh2*$^{fl/fl}$ group; therapeutic model, n= 25 mice for iCD4-Cre *Ezh2*$^{fl/fl}$ group and n= 28 mice for *Ezh2*$^{fl/fl}$ group.

Single-cell RNA sequencing (scRNA-seq) and single-cell T-cell receptor sequencing (scTCR-seq) of splenic CD4$^+$ T cells and kidney-infiltrating CD4$^+$ T cells

Spleens were mashed through 70-μm cell strainers with a syringe plunger and rinsed with PBS to prepare into single-cell suspensions. For kidney dissociation, we used the Multi Tissue Dissociation Kit 2 from Miltenyi Biotec and followed the protocol for mouse kidney dissociation. To preserve cell surface epitopes, we decreased the volume of Enzyme P in the dissociation buffer and the kit's components for each kidney were as follows: 4.8 mL of Buffer X, 5 μL Enzyme P, 50 μL Buffer Y, 100 μL Enzyme D, and 20 μL Enzyme A. Kidney capsules were removed, and kidneys were placed into gentleMACS C tubes (Miltenyi Biotec) with dissociation buffer and quartered. GentleMACS Octo Dissociator with heating function (Miltenyi Biotec) was used and the program '37C_Multi_E' was run to dissociate kidneys. Cell suspension went through a 70-μm cell strainer and was rinsed with PBS. Red blood cells (RBCs) in the spleens and kidneys were lysed with RBC lysis buffer (Invitrogen). Cells were resuspended in PBS and stained with LIVE/DEAD fixable near-IR dead cells stain kit (Thermo Fisher Scientific). Then cells were blocked with anti-mouse CD16/CD32 (BD Biosciences) followed by staining with the following antibodies: anti-CD3 epsilon-VioBlue (Clone 17A2, Miltenyi Biotec), anti-TCR β-Alexa Fluor 488 (Clone H57-597, BioLegend), anti-CD4-Pacific Green (Clone RM4-5, Thermo Fisher Scientific), and anti-CD8a-PE-Cyanine5 (Clone 53-6.7, BioLegend) in PBS with 1% fetal bovine serum (FBS). CD4$^+$ T cells from a total of 10 *Ezh2*$^{fl/fl}$ mice and 9 iCD4-Cre *Ezh2*$^{fl/fl}$ mice were sorted by FACSAria cell sorter in the Unified Flow Core at the Department of Immunology in the University of Pittsburgh.

CD4$^+$ T cells isolated from a single organ in each mouse were individually incubated with unique TotalSeq-C anti-mouse antibodies from BioLegend. All CD4$^+$ T cells were barcoded to distinguish between different organs and mice before pooling cells together. Sequencing libraries of cell surface protein feature barcoding, single cell 5' gene expression, and paired single-cell T-cell receptor (TCR) were prepared according to instructions provided by10x Genomics in the Single Cell Core at the University of Pittsburgh. These libraries were sequenced at the UPMC Genome Center. In total, 10,271 splenic CD4$^+$ T cells from *Ezh2*$^{fl/fl}$ mice were sequenced, with a mean of 26,854 reads per cell, and 7,704 splenic CD4$^+$ T cells from iCD4-Cre *Ezh2*$^{fl/fl}$ mice were sequenced with a mean of 22,603 reads per cell. In the kidneys,

8,850 kidney-infiltrating CD4$^+$ T cells from *Ezh2*$^{fl/fl}$ mice were sequenced, with a mean of 24,796 reads per cell, and 4,066 kidney-infiltrating CD4$^+$ T cells from iCD4-Cre *Ezh2*$^{fl/fl}$ mice were sequenced with a mean of 25,649 reads per cell.

Single-cell sequencing data analysis

Cell Ranger v. 7.1.0 (10x Genomics, Pleasanton, CA, USA) was used to process raw sequencing data following the 10x instructions (https://www.10xgenomics.com/analysis-guides/demultiplexing-and-analyzing-5'-immune-profiling-libraries-pooled-with-hashtags). Briefly, gene expression and T-cell receptor data were demultiplexed with 'cellranger multi' and organ-specific data were aggregated using 'cellranger aggr'. Gene expression data analysis was performed using Seurat v.5.0.1 R package following the standard workflow for visualization and clustering ("Seurat - Guided Clustering Tutorial" vignette). Clustering resolution ("resolution" parameter in the FindClusters function) was set to 0.5 to obtain biologically expected number of clusters. Cluster-specific conserved markers were detected using the FindConservedMarkers function. Clusters were annotated using scTyper v.0.1.0,[20] singleR v.2.4.1,[21] clustermole v.1.1.1 and manually annotated based on cluster-specific differentially expressed genes. Selected clusters were merged to represent major cell types (for kidney data, two clusters were merged into "Activated naïve CD4$^+$ T cells" and three clusters were merged into "Effector CD4$^+$ T cells"; for spleen, two clusters were merged into "Memory CD4$^+$ T cells"). Immune receptor sequencing data for each condition were annotated with cluster-specific barcodes defined at the RNA-seq analysis step and analyzed using the scRepertoire v.1.12.0 R package. Plots were made using Seurat's visualization functions or the ggplot2 v3.4.4 R package. All computations were performed in R/Bioconductor v.4.3.2.

Flow cytometry analysis of CD4$^+$ T cells

Single-cell suspensions obtained from the spleens and kidneys after RBC lysis were used to characterize CD4$^+$ T cells. LIVE/DEAD fixable near-IR dead cells stain kit (Thermo Fisher Scientific) was used and anti-mouse CD16/CD32 (BD Biosciences) was added to decrease non-specific bindings. The following antibodies were incubated with the cells at 4°C for 30 minutes: anti-CD3 epsilon-VioBlue (Clone 17A2, Miltenyi Biotec), anti-TCR β-Alexa Fluor 488 (Clone H57-597, BioLegend), anti-CD4-Pacific Green (Clone RM4-5, Thermo Fisher Scientific), anti-CD8a-PE-Cyanine5 (Clone 53-6.7, BioLegend), anti-CD44-Alexa Fluor 647 (Clone IM7, BioLegend), anti-CD62L-PE/Cyanine7 (Clone MEL-14, BioLegend), and anti-CD279 (PD1)-PE-Dazzle 594 (Clone RMP1-30, BioLegend). Cells were incubated with anti-CD185 (CXCR5)-PerCP/Cyanine5.5 (Clone L138D7, BioLegend) at room temperature for 1 hr, and True-Nuclear Transcription Factor Buffer Set (BioLegend) was used to fix and permeabilize cells before staining with anti-FoxP3-PE (Clone REA788, Miltenyi Biotec). Cell events were recorded with LSRFortessa (BD Biosciences) at the Department of Pediatrics, University of Pittsburgh, and Flowjo (BD Biosciences) was used for data analysis. The following number of mice were used for flow cytometry experiments to assess T cell subsets: spleen (preventative model), n= 19 mice for iCD4-Cre *Ezh2*$^{fl/fl}$ group and n= 18 mice for *Ezh2*$^{fl/fl}$ group; spleen (therapeutic model), n= 19 mice for iCD4-Cre *Ezh2*$^{fl/fl}$ group and n= 20 mice for *Ezh2*$^{fl/fl}$ group; kidney (preventative model), n= 19 mice for iCD4-Cre *Ezh2*$^{fl/fl}$ group and n= 18 mice for *Ezh2*$^{fl/fl}$ group.

QUANTIFICATION AND STATISTICAL ANALYSIS

Data were presented as either mean ± standard deviation (SD) or median ± interquartile range. Mann-Whitney *U* test was primarily used to compare differences between groups in GraphPad Prism 9.2.0 (GraphPad, San Diego, CA, USA). A *p* value less than 0.05 was considered statistically significant. Details of the specific statistical tests used in every experiment are indicated in the figure legends. Significance levels (*P* values) are indicated in the legend of each figure, showing *p<0.05, **p<0.01, ***p<0.001, ****p<0.0001, and non-significant comparisons are not marked. In the figure legends, "n" where mentioned indicates the number of animals.